

A Novel Glucose Biosensor Fabricated with Electroactive Nb_{0.95}Ti_{0.95}O₄ Nano-Composite Film

He Li^{1,*}, Xianwei Huang¹, Junli Lu¹, Fang Sun¹, Fenyun Yi¹, Yu Wang^{2,*}, Youwen Tang¹

¹ School of Chemistry and Environment, South China Normal University, Guangzhou 510006, China

² Department of Pathology, Zhujiang Hospital, Southern Medical University, Guangzhou 510282, China

*E-mail: lihelab@gmail.com (He Li) ; doctorwylh@163.com (Yu Wang)

Received: 6 August 2012 / Accepted: 5 September 2012 / Published: 1 October 2012

A novel Nb_{0.95}Ti_{0.95}O₄ (NTO) nanoparticle was synthesized and successfully fabricated in enzyme biosensors by integrating glucose oxidase (GOx) with a chitosan-Nb_{0.95}Ti_{0.95}O₄ (CHIT-NTO) nanocomposite onto an indium-tin-oxide (ITO) electrode. The results reveal that the presence of NTO can enhance electron transfer and increase the electroactive surface area between GOx and the ITO electrode. This mainly attributes to substitution of Ti⁴⁺ by Nb⁵⁺ to form ionization of defects improving its electrical conductive property. The NTO-modified bioelectrode exhibits an excellent linear range, low detection limit and long shelf life. The results suggest that CHIT-NTO is a promising material for biosensor electrode.

Keywords: Nb_{0.95}Ti_{0.95}O₄ nanoparticles Chitosan Glucose oxidase Biosensor

1. INTRODUCTION

Amperometric enzyme biosensors have recently received attention because of their potential applications in biological and chemical analysis, clinical detection, environmental monitoring, food and safety/security control [1-3]. Highly sensitive, repeatable, stable and disposable enzyme biosensors are required in the diagnosis of diabetes in order to determine the glucose levels in blood and urine [4]. In the development of a biosensor with improved electrochemical response, enzyme attachment and its compatibility with a solid surface are crucial factors [5]. A wide variety of electrode-modifying materials and techniques have been developed to achieve these key parameters [6-8]. However, the search for novel materials to further improve electrochemical biosensors remains paramount.

A number of metal oxide nanoparticles such as CeO₂ [9-12], ZnO [13-15], SnO₂ [16-17], Fe₃O₄ [18], ZrO₂ [19], NiO [20] and TiO₂ [21-24] have been found to exhibit interesting properties such as

large surface-to-volume ratio, high surface reaction activity, high catalytic efficiency, non-toxicity and strong adsorption ability [25] that make them potential candidate materials for the fabrication of enzyme-based biosensors. Enzyme biosensors require direct electron transfer between the redox protein and the electrode for the three-dimensional structure of the protein hinders interaction [26].

Recently, combining the advantages of inorganic materials and organic polymers for the fabrication of biosensors has been reported. Chitosan (CHIT), a natural cationic polymer, in combination with metal oxide nanoparticles, has excellent film-forming ability, mechanical strength, biocompatibility, non-toxicity, high permeability towards water, susceptibility to chemical modification and cost-effectiveness, and has been used as a stabilizing agent for enzyme (GOx) immobilization [12,27]. The potential of combining ceramic materials and organic polymers as a composite matrix for GOx immobilization deserves investigation. Furthermore, doping TiO₂ nanoparticles with a small amount of donor-type ions, such as Nb, can provide excellent electronic conductivity along with the original characteristic properties of the metal oxide [28-29]. That is because titanium oxide can form nonstoichiometric compounds, which have different electrical properties than stoichiometric titanium oxide [30]. Nonstoichiometric compounds have additional electron level in band gap and exhibit semiconducting properties [31]. It is well known that its electrical properties are dominated by oxygen vacancies and impurities. It is highly desirable to chemically incorporate impurity atoms without changing the crystallographic structure.

In this study, in order to obtain excellent electrical conductive nanomaterial based on doping impurities, a novel Nb_{0.95}Ti_{0.95}O₄ nanoparticle was firstly synthesized and successfully used in glucose biosensors. Amperometric glucose biosensors were then fabricated by immobilization of the GOx enzyme on a nanoporous CHIT–NTO thin film deposited on an ITO-coated glass plate. The fabrication, characterization and analytical performance of the modified glucose biosensor based on CHIT–NTO are described below.

2. EXPERIMENTAL

2.1 Reagents

Ammonium niobate(V)oxalate hydrate, and tetrabutyl titanate were purchased from Sigma-Aldrich, USA; D-Glucose, GOx (>100U/mg), Chitosan(CHIT) were acquired from Amresco, USA. Nitric acid, citric acid, ammonium hydroxide, sodium dihydrogen phosphate and sodium hydrogen phosphate were obtained from Aladdin, China. All chemicals were used without further purification. Deionized water was used for the preparation of aqueous solutions.

The stock solution of GOx (1 mg/dL) was freshly prepared in phosphate buffer solution (50mM) at pH=7.0 and stored at 4°C. Different concentrations of glucose solution were freshly-prepared in deionized water.

2.2 Preparation of $Nb_{0.95}Ti_{0.95}O_4$ nanoparticles

6.0 g of citric acid ($C_6H_8O_7$) were dissolved in 200 mL of deionized water by heating and stirring at 80 °C. 5 mL of concentrated nitric acid solution were added after the citric acid had completely dissolved. 3.5 mL of tetrabutyl titanate solution was then added, with constant stirring, for 2 h at 80~100 °C, generating a clear solution. Ammonium hydroxide (NH_4OH) was added until a neutral pH was achieved, prior to dissolving 3.0 g of ammonium niobate (V) oxalate hydrate in the solution, with stirring for 1~2h, at 80~100 °C. A swollen black sample, obtained by placing the solution into an oven at 200°C ~250°C, was sintered at 900 °C for 5 h to generate nanoparticles of NTO.

2.3 Preparation of the CHIT–NTO/ITO nanocomposite electrodes

0.5% CHIT solution was prepared by dissolving 10 mg CHIT in 2.0 mL of acetate buffer (0.05 M, pH 4.2) solution. 2 mg of NTO was ultrasonically dispersed as nanoparticles in the CHIT solution, requiring more than 1h due to the high viscosity of the resulting solution. 10 μ L of the CHIT–NTO solution was then transferred onto a 0.25 cm² ITO surface and allowed to dry at room temperature overnight in a controlled environment. The CHIT–NTO nanocomposite film was then washed with deionized water to remove any unbound particles.

2.4 Immobilization of GOx onto the CHIT–NTO/ITO electrode

Immobilization of GOx onto the CHIT–NTO matrix was achieved by utilizing the electrostatic interaction between positively-charged CHIT and the negatively-charged GOx enzyme. 10 μ L of freshly-prepared GOx solution (1mg/dL) was spread onto the CHIT–NTO/ITO electrode; the resulting GOx/CHIT–NTO/ITO bioelectrode was kept undisturbed for about 12 h at 4 °C. Prior to washing with 50 mM PBS (pH 7.0), in order to remove any unbound GOx from the electrode surface, then kept at 4 °C when not in use.

2.5 Characterization

The phase of the NTO nanoparticles was determined by X-ray diffraction (XRD, D8 ADVANCE, Bruker AXS). The NTO, CHIT–NTO/ITO electrode and GOx/CHIT–NTO/ITO bioelectrodes were investigated using Fourier transform infrared spectroscopy (FTIR, Prestige-21, SHI-MADZU) and atomic force field emission scanning electron microscopy (SEM, JSM-6330F, JEOL). Electrochemical analysis was conducted on an Autolab Potentiostat/Galvanostat (PGSTAT-30, Eco Chemie, Netherlands) using a three-electrode system with ITO as the working electrode, platinum (Pt) as the auxiliary electrode, and Ag/AgCl as the reference electrode in a phosphate buffer saline (PBS) solution (50 mM, pH 7.0, 0.9% NaCl) containing 5mM $[Fe(CN)_6]^{3-/4-}$ as the redox probe.

3. RESULTS AND DISCUSSION

3.1 XRD analysis

Fig.1-I shows the XRD pattern of NTO nanoparticles. All the XRD peaks were consistent with the peaks of $\text{Nb}_{0.95}\text{Ti}_{0.95}\text{O}_4$ (PDF card No.47-0024). No other impurity phase was detected by XRD analysis.

3.2 FTIR

The FTIR spectra of NTO nanoparticles exhibited a sharp, intense peak at 518 cm^{-1} , which may be attributed to the bonding of Nb-O-Ti (Fig. 1-II).

The IR spectra of Fig. 1-III illustrate the contrast between CHIT, CHIT-NTO, GOx and the GOx/CHIT-NTO/ITO bioelectrode. Compared with curve (a), the characteristic IR bands of the functional group corresponding to pure CHIT: the hydroxyl group, amido group ($3450, 1600, 1099\text{ cm}^{-1}$), amide group (C-O stretching along with N-H deformation mode 1640 cm^{-1}), C-N axial deformation (amine group band 1426 cm^{-1}) [32] and Nb-O-Ti bond (518 cm^{-1}) were all exhibited in curve b for the CHIT-NTO nanocomposite. The presence of CHIT in the CHIT-NTO composite facilitates immobilization of biomolecules *via* the amine and hydroxyl groups. The FTIR spectrum of the GOx/CHIT-NTO bioelectrode (curve d) exhibits the characteristic infrared bands of GOx (curve c) and the CHIT-NTO nanocomposite (curve b), demonstrating the immobilization of GOx on the nanocomposite matrix (overlapped peaks at 1640 and 1439 cm^{-1}).

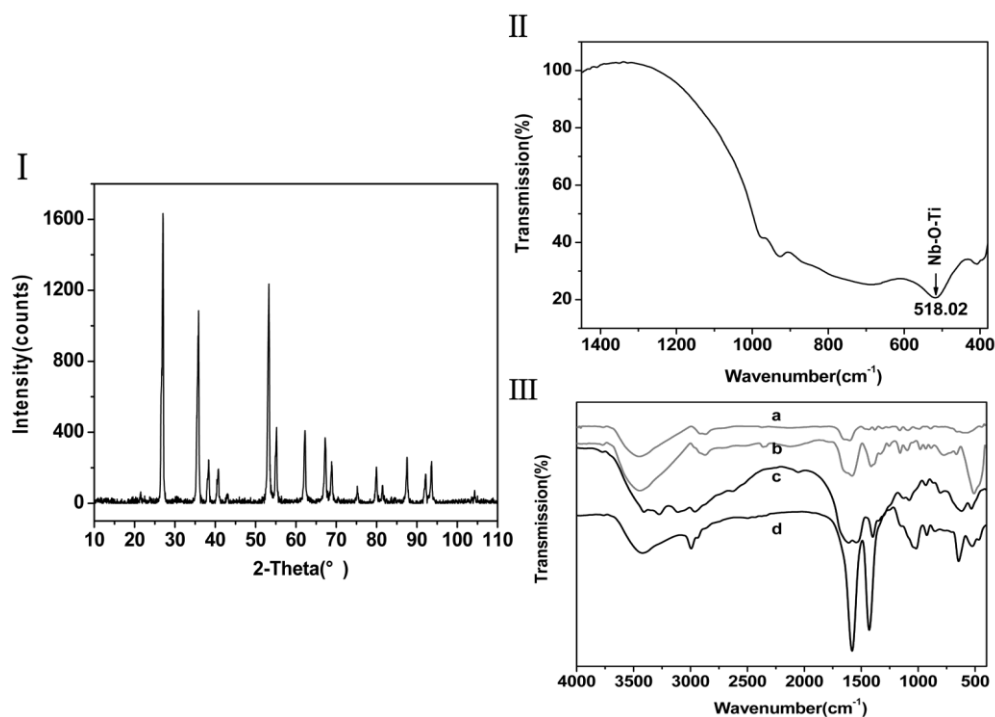


Figure 1. I) The X-ray diffraction pattern of NTO nanoparticles, II) FTIR spectra of $\text{Nb}_{0.95}\text{Ti}_{0.95}\text{O}_4$, III) FTIR spectra of (a) CHIT; (b) CHIT-NTO nanocomposite; (c) GOx; (d) GOx/CHIT-NTO/ITO bioelectrode.

3.3 Surface morphology studies

Fig. 2 presents SEM images illustrating the surface morphologies of the electrodes: (a) NTO/ITO; (b) CHIT/ITO; (c) CHIT–NTO/ITO; (d) GOx/CHIT–NTO/ITO. The SEM image of NTO/ITO exhibits granular morphology with an average grain size of about 30–50 nm. Fig.2-b shows that the thin film of CHIT spread evenly in the surface of ITO electrode. The globular morphology of the CHIT–NTO/ITO electrode is revealed in Fig.2-c, indicating the formation of a CHIT–NTO hybrid nanocomposite, which may be attributed to electrostatic interactions between the cationic CHIT and a surface charge on the NTO nanoparticles. The granular lacunar surface of the CHIT–NTO film is suitable for the immobilization of biomolecules. The surface morphology of GOx/CHIT–NTO/ITO assumes a well-regulated form (Fig. 2-d) once GOx has been firmly immobilized onto the CHIT–NTO/ITO electrode by electrostatic interactions.

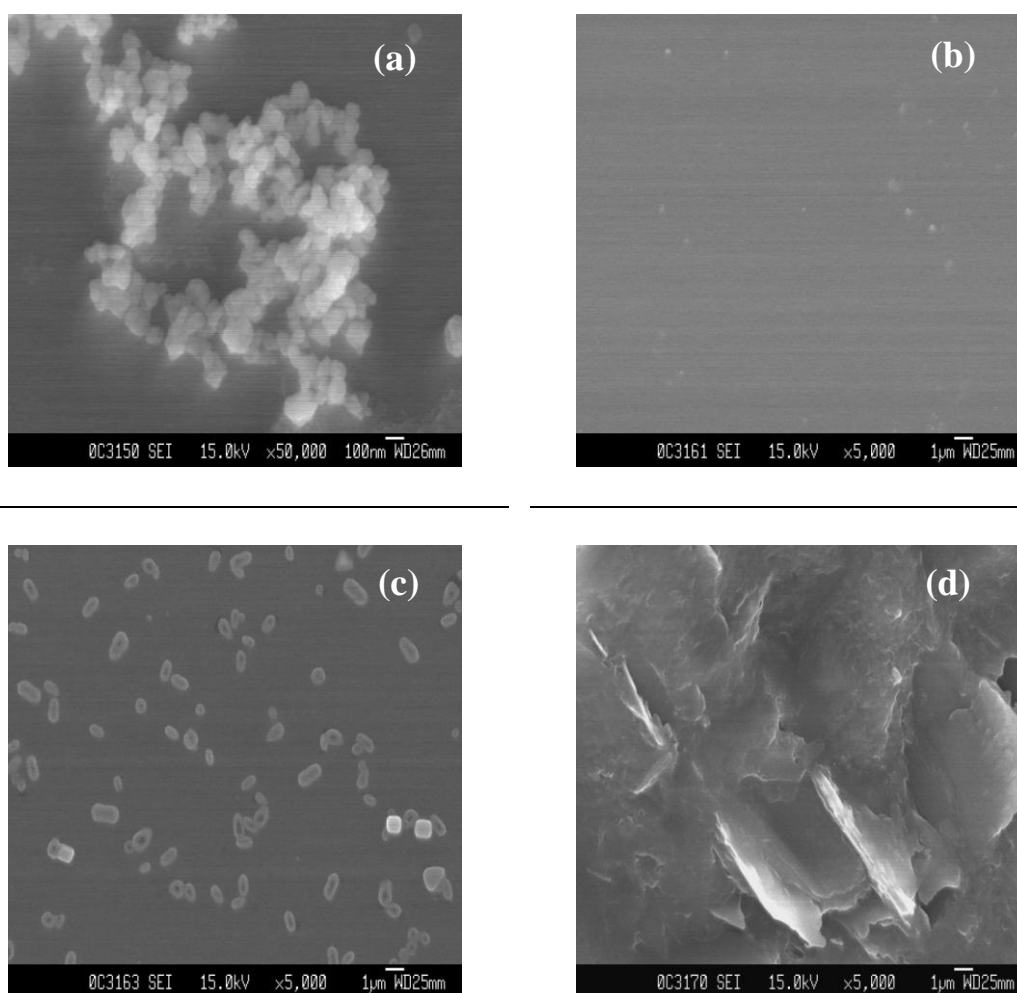


Figure 2. SEM images of: (a) the NTO/ITO electrode; (b) the CHIT/ITO electrode; (c) the CHIT–NTO/ITO electrode; (d) the GOx/CHIT–NTO/ITO bioelectrode.

3.4 Electrochemical studies

Fig. 3-I illustrates the results of cyclic voltammetric (CV) studies conducted on various ITO-modified electrodes immersed in PBS in the potential range -0.4 to 0.8 V at a 10 mV/s scanning rate. The increase in magnitude of the current for the CHIT/ITO electrode (curve b) as compared to the ITO electrode (curve a) may be due to the acceptance of electrons from the negatively-charged ferricyanide species in the PBS by cationic CHIT, resulting in an enhanced redox current[32]. The additional increase in magnitude of the current response for the CHIT–NTO/ITO electrode (curve c) suggests that the presence of NTO nanoparticles increases electroactive surface area and therefore enhances electron transfer. This mainly attributed to substitution of Ti^{4+} by Nb^{5+} to form ionization of defects. After the immobilization of GOx onto the electrodes, the CHIT–NTO/ITO electrode (curve e) has a higher peak current than the CHIT/ITO electrode, indicating that the CHIT–NTO/ITO electrode accelerates electron transfer between GOx and the electrode.

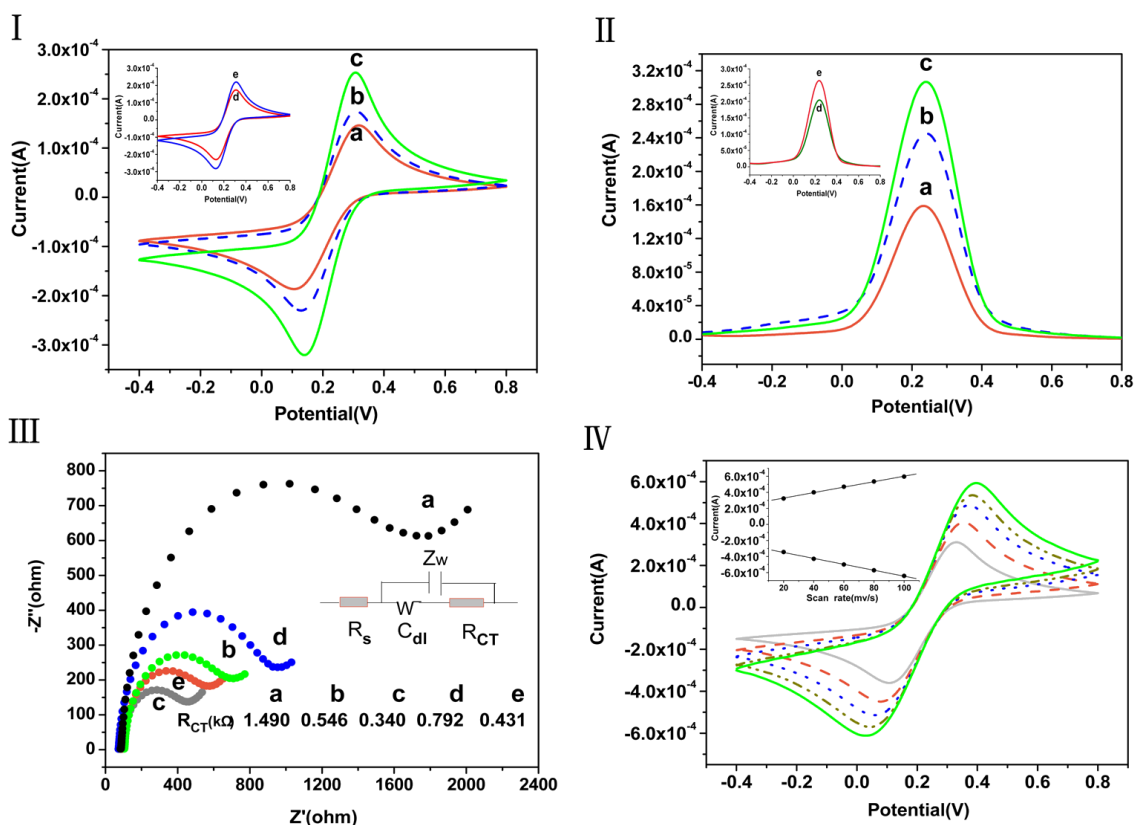


Figure 3. I) Cyclic voltammograms of the test electrodes: (a) ITO; (b) CHIT/ITO; (c) CHIT–NTO/ITO; II) Differential pulse voltammograms (DPV) of the test electrodes: (a) ITO; (b) CHIT/ITO; (c) CHIT–NTO/ITO; (inset for bioelectrodes: (d) GOx/CHIT/ITO; (e) GOx/CHIT–NTO/ITO.) III) Electrochemical impedance spectroscopy of the test electrodes: (a) ITO; (b) CHIT/ITO; (c) CHIT– $Nb_{0.95}Ti_{0.95}O_4$ /ITO; and bioelectrodes (d) GOx/CHIT/ITO; (e) GOx/CHIT– $Nb_{0.95}Ti_{0.95}O_4$ /ITO; inset: equivalent circuit; IV) Cyclic voltammograms of the GOx/CHIT– $Nb_{0.95}Ti_{0.95}O_4$ /ITO bioelectrode at scan rates of 20 – 100 mV/s, inset: magnitude of the current as a function of scan rate.

Fig. 3-II presents differential pulse voltammograms (DPV) of the various ITO-modified electrodes in PBS. The presence of cationic CHIT allows acceptance of electrons from the medium and transference of these to the electrode, and the uniform dispersion of NTO nanoparticles throughout the CHIT network promote electron transfer due to the generation of surface oxygen vacancies. Also, the increased magnitude of the response of the CHIT–NTO/ITO bioelectrode (curve e) suggests that the presence of NTO provides a favorable environment for the immobilization of GOx, resulting in enhanced electron transfer.

Electrochemical impedance spectroscopy (EIS) has been demonstrated to be an effective method for the study of the interfacial properties of surface-modified electrodes [33,34]. Fig. 3-III presents the EIS of surface-modified electrodes obtained at open potential along with the equivalent circuit in the frequency range of $10^5 \sim 10^{-2}$ Hz. In EIS, the total impedance is determined by various parameters, including solution resistance (R_s), double layer capacitance (C_{dl}), charge transfer resistance (R_{CT}) and Warburg element (Z_w) [9]. The R_s and Z_w values, representing the resistance of the electrolyte solution and the diffusion of the applied redox probe, are not affected by biochemical reactions occurring at the electrode interface. C_{dl} and R_{CT} , however, are dependent upon the dielectric and insulating features at the electrode/electrolyte interface [35]. The semicircular portion of the EIS curve corresponds to an electron transfer-limited process and its diameter is equal to the electron transfer resistance, R_{CT} , which controls the electron transfer kinetics of the redox probe at the electrode interface.

The diameter of the semicircle, R_{CT} , the characteristic of the diffusion limiting step of the electrochemical process, is 1.490 K Ω for the ITO electrode (curve a in Fig3-III), decreases to 0.546 K Ω with the addition of CHIT (curve b in Fig3-III) and further decreases to 0.340 K Ω when NTO is incorporated (curve c in Fig3-III). Similarly, for the bioelectrodes, R_{CT} decreases from 0.792 K Ω (curve d) to 0.546 K Ω with the incorporation of NTO (curve e). The electron transfer resistance decreases in the order: bare ITO > GOx/CHIT/ITO > CHIT/ITO > GOx/CHIT-NTO/ITO > CHIT-NTO/ITO, implying easier electron transfer between the solution and the electrode in the CHIT–NTO nanocomposite film; NTO nanoparticles provide increased electroactive surface, plus promote electron transfer between the electrode and GOx. However, the GOx layer acts as a barrier for electron transfer between the electrode surface and the redox probes in the solution, which confirms the immobilization of GOx onto the CHIT/ITO and CHIT–NTO/ITO electrodes [1], presumably due to the insulating characteristics of glucose oxidase.

Fig. 3-IV exhibits cyclic voltammograms of the GOx/CHIT–NTO/ITO bioelectrode in PBS (pH 7.0) as a function of scan rate (from 10 to 100mV/s). Anodic (I_a) and cathodic (I_c) currents are linearly proportional to the scan rate (inset, Fig. 3-IV) according to Eqs. (1) and (2), which show a typical diffusion-controlled electrochemical behavior.

$$I_a (A)_{(CH-nanoNb_{0.95}F_{1.05}O_2/ITO)} = 2.605 \times 10^{-4} A + 3.405 \times 10^{-6} A \times \nu \quad (1)$$

where ν is scan rate (mV/s); the square of the correlation coefficient, $R^2 = 0.997$

$$I_c(A)_{(GO_x/CH-nanoNb_{0.95}Ti_{0.05}O_2/ITO)} = -2.757 \times 10^{-4} A - 3.695 \times 10^{-6} A \times \nu \tag{2}$$

where ν is scan rate (mV/s), and $R^2 = 0.998$

The surface concentration of the GOx/CHIT–NTO/ITO bioelectrode has been estimated using Eq (3):

$$I_p = 0.227nFAC^*_0 \times k^0 \exp \left[\frac{-\alpha n_a F}{RT} (E_p - E^{\theta'}) \right] \tag{3}$$

where I_p is the anodic peak current, n is the number of electrons transferred (1), F is the Faraday constant ($96485.34 \text{ C}\cdot\text{mol}^{-1}$), A is the surface area (0.25 cm^2), R is the gas constant ($8.314 \text{ J}\cdot\text{mol}^{-1}\cdot\text{K}^{-1}$), C^*_0 is the surface concentration of ionic species on the film surface ($\text{mol}\cdot\text{cm}^{-2}$), E_p is the peak potential and $E^{\theta'}$ is the formal potential. $(-\alpha n_a F/RT)$ and k_0 (rate constant) correspond to the slope and intercept of the $\ln(I_p) \text{ vs } E_p - E^{\theta'}$ curve at different scan rates. The addition of NTO nanoparticles increases the surface concentration of GOx by an estimated $9.91 \times 10^{-6} \text{ mol cm}^{-2}$ higher.

The effect of pH on the GOx/CHIT–NTO/ITO bioelectrode was investigated using CV (Fig. 4-I) and DPV (Fig. 4-II) techniques in PBS (50mM) containing $5\text{mM}[\text{Fe}(\text{CN})_6]^{3-/4-}$ at a scan rate of 10mV/s . Insets in Figs. 4-I and 4-II present the calibration curves obtained as a function of pH from 6 to 8. The current increases in the pH range from 6.0 to 7.0, while decreasing in the range from 7.0 to 8.0, suggesting that GOx retains its natural structure in the neutral state, resulting in enhanced interaction between the redox ions and the bioelectrode surface.

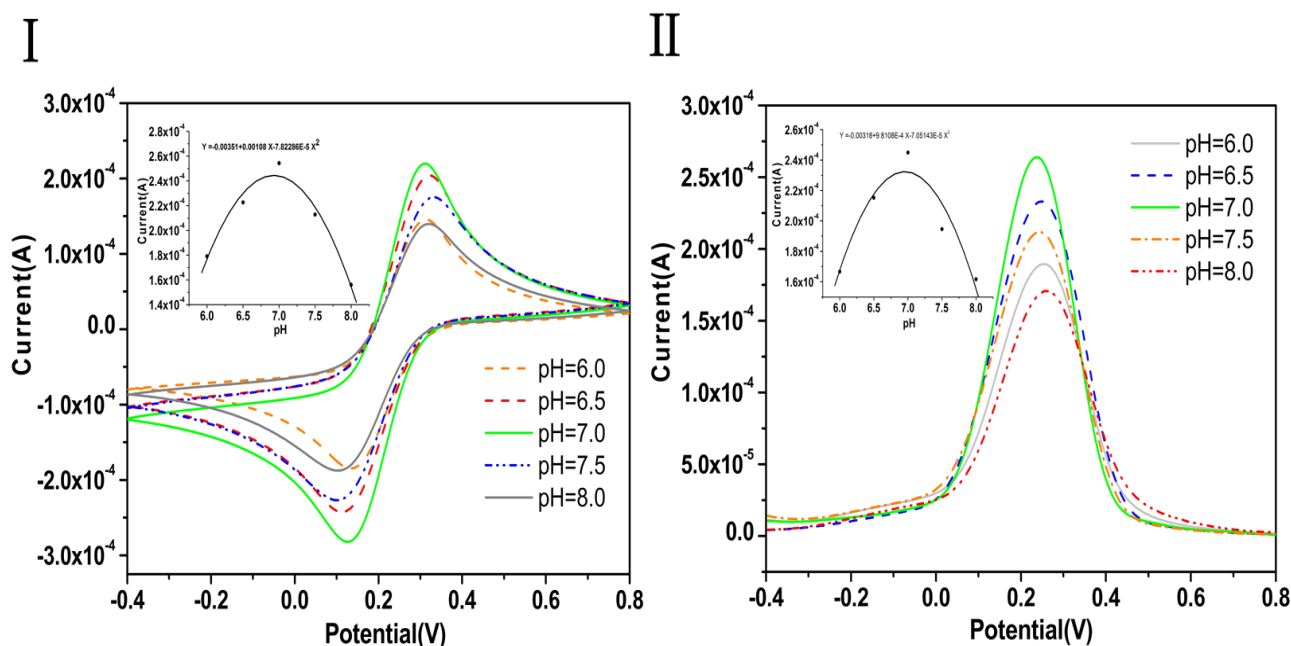


Figure 4. I) CV curves of the GOx/CHIT–NTO/ITO bioelectrode for pH = 6.0 - 8.0 at a scan rate of 10mV/s . (Inset shows the effect of pH on the bioelectrode.); II) Differential pulse voltammetry of the GOx/CHIT–NTO/ITO bioelectrode as a function of pH (6.0 - 8.0).

3.5 Electrochemical response studies

The electrochemical response of the GOx/CHIT–NTO/ITO bioelectrode was investigated as a function of glucose concentration (100 μL of 10 – 400 mg dL^{-1}) using the CV technique (Fig. 5-I) at a scan rate of 10 mV/s in PBS (50 mM , pH 7.0, 0.9%NaCl) containing 5 mM $[\text{Fe}(\text{CN})_6]^{3-/4-}$. The response current increases with increasing glucose concentration; this can be attributed to the presence of CHIT–NTO nanocomposite which accepts electrons during the reoxidation of GOx and transfers them to the electrode, effectively acting as an electron transfer-accelerating layer. The inset in Fig. 5-I shows the variation of peak response current with glucose concentration. The low detection limit, fast response time and high sensitivity are 0.5 mM , 8s, and 1.29 $\text{mA/mg dL}^{-1} \text{cm}^2$, respectively.

The Michaelis-Menten kinetic parameter (Kappm) of enzymatic reaction, which determines the affinity of enzyme (GOx) for its substrate, was estimated for the GOx/CHIT–NTO/ITO bioelectrode to be 0.629 mM (with a regression coefficient of 0.998) using a Hanes plot (Fig. 5-II) (substrate concentration as x axis and substrate concentration/current as y axis) [25, 36].

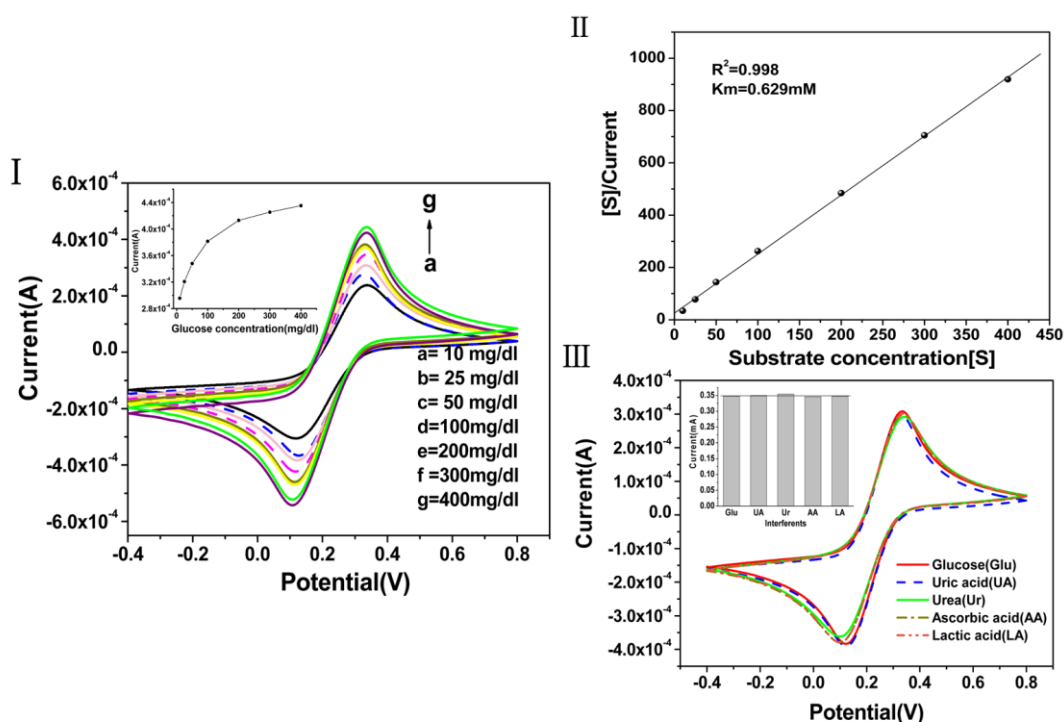


Figure 5. Electrochemical response studies of the GOx/CHIT–NTO/ITO bioelectrode: **I)** Current as a function of glucose concentration, using CV, Inset: calibration curve of current vs glucose concentration (10–400 mg.dL^{-1}). **II)** Hanes plot of [S]/current vs substrate concentration. **III)** Effect of contaminants on the GOx/ CHIT–NTO/ITO bioelectrode CV response.

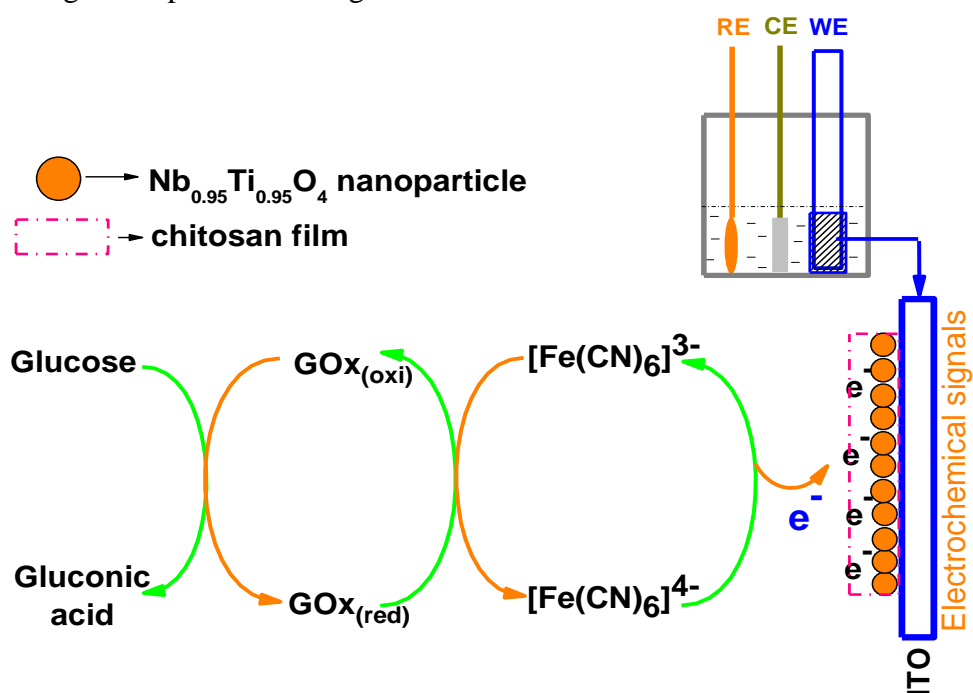
The observed low Kappm value reveals the enhanced affinity of GOx for its substrate. It can be seen that the low value of Kappm in the present investigations for glucose (Table 1) indicates the advantage of CHIT–NTO nanocomposite as compared to other oxides or polymer matrices for enzyme

immobilization. Favorable orientation provides a suitable microenvironment for effective immobilization of enzyme (GOx), and a higher loading of GOx on the enhanced surface area of the nanocomposite film, which also allows fast electron communication between the enzyme's active site and electrode.

Table 1. Comparison of the GOx/CHIT–Nb_{0.95}Ti_{0.95}O₄/ITO bioelectrode with those reported in literatures.

Immobilization matrix	Method of immobilization	Detection range	Detection limit	Km	Shelf-life	References
Gold nanoparticles	Covalent	50-	-	3.74 mM	180 days	[13]
macroporous TiO ₂	Physical	300mg/dL	0.02 mM	1.4 mM	10 days	[37]
CeO ₂	Physical	0.05-2.5	-	1.01mM	10 weeks	[5]
CHIT/NiFe ₂ O ₄ NPs	Physical	mM	-	-	>30 days	[1]
CHIT–Nb _{0.95} Ti _{0.95} O ₄	Physical	25– 300mg/dL 0.1–20mM 10- 400mg/dL	0.5mM	0.629mM	>10 weeks	Present work

Scheme 1 shows a proposed mechanistic pathway for electron generation in the biochemical reaction at the GOx/CHIT–NTO/ITO bioelectrode during glucose detection, wherein GOx hydrolyses glucose, resulting in the production of gluconic acid.



Scheme 1. Schematic of the electrochemical reaction at the surface of the GOx/ CHIT–NTO/ITO bioelectrode.

The reproducibility of the GOx/CHIT–NTO/ITO bioelectrode was investigated at 100 mg/dL glucose concentration, and no significant change in the current response was observed after at least 15 uses. When not in use, the electrode was stored dry at 4 °C in a refrigerator. Long term stability is an important criterion for a biosensor; the electrochemical current response of the GOx/CHIT–NTO/ITO bioelectrode in glucose solution was measured at a regular interval of 2 week, and retained more than 90% of the GOx activity after 6 weeks; thereafter, the current response decreased to 80% after 10 weeks, indicating a good stability.

The selectivity of GOx/CHIT–NTO/ITO bioelectrode was investigated by determining the amperometric response when normal concentrations (physiological range) of interferents (Fig. 5-III) such as uric acid (0.1 mM), urea (1 mM), ascorbic acid (0.05 mM) and lactic acid (1 mM) were added in equal concentration with that of glucose. The value of the electrochemical current response was virtually unchanged, demonstrating that the GOx/CHIT–NTO/ITO bioelectrode was not significantly affected by the presence of interferents, and demonstrates excellent selectivity.

4. CONCLUSIONS

A novel chitosan-NTO thin film was used to immobilize GOx by physisorption for glucose detection. The CHIT-NTO demonstrated excellent electronic conductivity as well as good biocompatibility, and maintains the biological activity of the enzyme plus enhances electron transfer between glucose and the GOx/ CHIT - NTO/ITO electrode surface. The fabricated glucose biosensor exhibits fast amperometric response, high sensitivity, a low detection limit, high selectivity, and long-term stability. Furthermore, the low K_{app} value (0.629mM) indicates a high affinity of the GOx/ CHIT - NTO/ITO bioelectrode for glucose. These results demonstrate that the CHIT -NTO nanocomposite could be readily extended to the fabrication of efficient amperometric biosensors for the detection of other clinically important antigens, and for other biological applications.

ACKNOWLEDGEMENTS

All the authors thank the Science and Technology Planning Project of Guangzhou (2009Z2-D511), and the Natural Science Foundation of Guangdong Province (No: 10151063101000011 and S2011040003162), China, for financial support.

References

1. L.Q. Luo, Q.X. Li, Y.H. Xu, Y.P. Ding, X. Wang, D.M. Deng and Y.J. Xu, *Sens. Actuators B* 145 (2010) 293.
2. S.F. Wang, Y.M. Tan, D.M. Zhao and G.D. Liu, *Biosens. Bioelectron.*, 23 (2008) 1781.
3. Y.C. Fu, C. Chen, Q.J. Xie, X.H. Xu, C. Zou, Q.M. Zhou, L. Tan, H. Tang, Y.Y. Zhang and S.Z. Yao, *Anal. Chem.*, 80 (2008) 5829.
4. C.C. Li, Y.L. Liu, L.M. Li, Z.F. Du, S.J. Xu, M. Zhang, X.M. Yin and T.H. Wang, *Talanta*, 77 (2008) 455.

5. S. Saha, S.K. Arya, S.P. Singh, K. Sreenivas, B.D. Malhotra and V. Gupta, *Biosens. Bioelectron.*, 24 (2009) 2040.
6. A.I. Gopalan, K.P. Lee, D. Ragupathy, S.H. Lee and J.W. Lee, *Biomaterials*, 30 (2009) 5999.
7. J.D. Qiu, R. Wang, R.P. Liang and X.H. Xia, *Biosens. Bioelectron.*, 24 (2009) 2920.
8. K.M. Manesh, J.H. Kim, P. Santhosh, A.I. Gopalan, K.P. Lee and H.D. Kang, *J Nanosci. Nanotech.*, 17 (2007) 3665.
9. A.A. Ansari, A. Kaushik, P.R. Solanki and B.D. Malhotra, *Electrochem. Commun.*, 10(2008) 1246.
10. J.A. Rodriguez, S. Ma, P. Liu, J. Hrbek, J. Evans and M. Perez, *Science*, 318(2007) 1757.
11. D.A. Andersson, S.I. Simak, N.V. Skorodumova, I.A. Abrikosov and B. Johansson, *Appl. Phys. Lett.*, 90(2007) 031909.
12. K.J. Feng, Y.H. Yang, Z.J. Wang, J.H. Jiang, G.L. Shen and R.Q. Yu, *Talanta*, 70(2006) 561.
13. P. Pandey, S.P. Singh, S.K. Arya, V. Gupta, M. Datta, S. Singh and B.D. Malhotra, *Langmuir*, 23(2007) 3333.
14. A. Wei, X.W. Sun, J.X. Wang, Y. Lei, X.P. Cai, C.M. Li, Z.L. Dong and W. Huang, *Appl. Phys. Lett.*, 89(2006) 123902.
15. S.F. Wang, Y.M. Tan, D.M. Zhao and G.D. Liu, *Biosens. Bioelectron.*, 23(2008) 1781.
16. C.W. Liao, J.C. Chou, T.P. Sun, S.K. Hsiung and J.H. Hsieh, *IEEE Trans. Biomed. Eng.*, 53(2006) 1401.
17. N. Jia, Q. Zhou, L. Liu, M.M. Yan and Z.Y. Jiang, *J. Electroanal. Chem.*, 580 (2005) 213.
18. L.Q. Yang, X.L. Ren, F.Q. Tang and L. Zhang, *Biosens. Bioelectron.*, 25 (2009) 889.
19. H. Kim, S.H. Yoon, H.N. Choi, Y. Lyu and W. Lee, *Bull. Korean Chem. Soc.*, 27 (2006) 65.
20. C.C. Li, Y.L. Liu, L.M. Li, Z.F. Du, S.J. Xu, M. Zhang, X.M. Yin and T.H. Wang, *Talanta*, 77 (2008) 455.
21. F.H. Wu, J.J. Xua, Y. Tian, Z.C. Hu, L.W. Wang, Y.Z. Xian and L.T. Jin, *Biosens. Bioelectron.*, 24 (2008) 198.
22. M. Viticoli, A. Curulli, A. Cusma, S. Kaciulis, S. Nunziante, L. Pandolfi, F. Valentini and G. Padeletti, *Mater. Sci. Eng. C*, 26 (2006) 947.
23. J. Yu and H. Ju, *Anal. Chem.*, 74 (2002) 3579.
24. Q. Li, G. Luo, J. Feng, Q. Zhou, L. Zhang and Y. Zhu, *Electroanalysis*, 13 (2001) 413.
25. P.R. Solanki, C. Dhand, A. Kaushik, A.A. Ansari, K.N. Sood and B.D. Malhotra, *Sens. Actuators B*, 141 (2009) 551.
26. G.C. Zhao, L. Zhang and X.W. Wei, *Anal. Biochem.*, 329 (2004) 160.
27. R. Khan, A. Kaushik, P.R. Solanki, A.A. Ansari, M.K. Pandey and B.D. Malhotra, *Anal. Chim. Acta*, 616 (2008) 207.
28. N.R. Elezovic, B.M. Babic, L.G. Krstajic, V. Radmilovic, N.V. Krstajic and L.J. Vracar, *J Power Sources*, 195 (2010) 3961.
29. J. Nowotny, T. Bak, M.K. Nowotny and L.R. Sheppard, *Int. J. Hydrogen. Energy*, 32 (2007) 2630.
30. A. Pavlova, J. Barloti, V. Teters, J. Locs and L. Berzina-Cimdina, *Process. Appl. Ceram.*, 3 (2009) 187.
31. M. Radecka, A. Tranczek-Zajac, K. Zakrzewska and M. Rekas, *J. Power Sources*, 173 (2007) 816.
32. B.D. Malhotra and A. Kaushik, *Thin Solid Films*, 518 (2009) 614.
33. Q.L. Sheng, Y. Shen, H.F. Zhang and J.B. Zheng, *Chin. J. Chem.*, 26 (2008) 1244.
34. E. Katz and I. Willner, *Electroanalysis*, 15 (2003) 913.
35. X. Chen, Y. Wang, J. Zhou, W. Yan, X. Li and J.J. Hu, *Anal. Chem.*, 80 (2008) 2133.
36. J.M. Walker, *Principles, Techniques of Practical Biochemistry*, 5th ed. 2000, Cambridge University Press, UK
37. H.M. Cao, Y.H. Zhu, L.H. Tang, X.L. Yang and C.Z. Li, *Electroanalysis*, 20 (2008) 2223.